

Exploring dynamical quantum phase transitions in a spin model with deconfined critical point via the quantum steering ellipsoid

Chang-Xiao Li, Sheng Yang , Jing-Bo Xu ,* and Hai-Qing Lin[†]

Zhejiang Institute of Modern Physics and School of Physics, Zhejiang University, Hangzhou 310027, China



(Received 16 December 2022; revised 8 February 2023; accepted 9 February 2023; published 21 February 2023)

The dynamical quantum phase transition (DQPT), which is featured by the nonanalytic behavior of the Loschmidt rate function in the real time evolution, has attracted substantial attention as a valuable theoretical concept for characterizing nonequilibrium states of quantum matter. Although the link between the DQPT and many physical concepts has been established, a thorough understanding of this transition still calls for more studies. In this paper, from the perspective of the quantum steering ellipsoid (QSE), we investigate the DQPTs supported in a one-dimensional spin chain with a deconfined quantum critical point by using the global subspace expansion time-dependent variational principle algorithm. For the quench from the valence-bond-solid phase to the ferromagnetic phase, we find a clear correspondence between the vanishing of the QSE volume and the occurrence of the DQPT. For the quench in the opposite direction, however, the QSE exhibits a rather complicated behavior during the time evolution. We also calculate the quantum entanglement and quantum coherence in the quench processes to unveil the change of the quantum correlations encoded in the QSE picture. These findings could offer a fascinating possibility of revealing DQPTs in a geometrically discernible manner.

DOI: [10.1103/PhysRevB.107.085130](https://doi.org/10.1103/PhysRevB.107.085130)

I. INTRODUCTION

With the high degree of experimental control in current ultracold-gas and condensed-matter settings [1–4], the study of nonequilibrium quantum many-body dynamics has been possible and attracted great attention among theorists and experimentalists. A natural focus of such experiments is the concept of dynamical quantum phase transitions (DQPTs) [5–7], which appear in the quench dynamics of a quantum system generated by the abrupt change of some global parameters in the Hamiltonian. Since the seminal work elaborating on this concept in the quantum transverse-field Ising model [6], theoretical studies demonstrating the relationship between DQPTs and other physical concepts like universality, order parameters, and topology [8–23], as well as pioneering experiments achieving DQPTs in ionic and atomic platforms [24,25], have made significant progress. In a common definition, DQPTs are signified by the nonanalyticities in the form of kinks in the Loschmidt rate function [6,7]

$$\lambda(t) = - \lim_{N \rightarrow \infty} \frac{1}{N} \ln |l(t)|^2, \quad (1)$$

in which N is the system size and $l(t) = \langle \psi(t) | \psi(0) \rangle$ is the Loschmidt amplitude that measures the overlap between the initial state $|\psi(0)\rangle$ and the time-evolved state $|\psi(t)\rangle = \exp(-iHt)|\psi(0)\rangle$ with H the quench Hamiltonian. Although the Loschmidt rate function is a reliable indication of DQPTs, it provides limited insight into the rich phenomenology associated with the nonequilibrium quantum

many-body dynamics. It still calls for further research from different perspectives to reveal more aspects of DQPTs, which is vital in elucidating the fundamental mechanism of quantum many-body systems in quench dynamics.

On the other hand, the deconfined quantum critical point (DQCP) is an intriguing concept that was initially proposed to support a direct continuous phase transition between a valence-bond-solid (VBS) phase and an antiferromagnetic Néel phase in two-dimensional (2D) quantum Heisenberg magnets with incompatible order parameters [26], which is forbidden by the Landau-Ginsberg-Wilson theory [27,28]. The DQCP theory was presented by showing that the predominant fluctuating modes near the critical point are deconfined spinons and emergent gauge fields; the VBS and Néel order parameters are composites of these deconfined degrees of freedom rather than fundamental objects themselves [29]. While elaborate effort has been put into the study of possible 2D lattice models [30–40], it remains disputed whether the relevant phase transitions are continuous or weakly first order. In contrast, recent theoretical and numerical studies [41–46] strongly suggested an analog of the DQCP in a 1D spin chain. This allows us to investigate the DQPT concept in the context of DQCP with powerful matrix-product-state (MPS) techniques [47–49].

Prior research on the DQPT in the 1D DQCP model mainly focused on the Loschmidt rate function and dynamical order parameters [50]. However, little is known about the underlying mechanism of these DQPTs or their relation to other physical quantities. Over the past several years, a convenient concept in quantum information, the quantum steering ellipsoid (QSE) [51], has been developed to describe two-qubit states. Its geometric properties can reflect many much-studied quantum correlations, such as quantum discord [51–53],

*xujb@zju.edu.cn

†hqlin@zju.edu.cn

quantum entanglement [54,55], and Einstein-Podolsky-Rosen steering [56,57]. Recently, it was demonstrated that QSE could characterize equilibrium quantum phase transitions in a geometric way [58]. Therefore, extending this approach to the nonequilibrium case is a possible research topic of interest. On the other hand, quantum entanglement has been employed to study a wide range of quantum many-body problems [59], especially the possibility of classifying DQPTs in the low-entanglement regime [18]. As a visualization tool encoding two-qubit quantum correlations, QSE can be a potential indication of DQPTs and provides a different perspective for nonequilibrium quantum many-body dynamics. Relevant experiments may be implemented using some well-developed techniques [60].

In this paper, motivated by the inspiration mentioned above, we use the QSE to study the DQPTs supported in the 1D DQCP chain proposed in Ref. [41]. We have considered two types of quench protocols by making use of the global subspace expansion time-dependent variational principle (GSE-TDVP) algorithm [61]. For the quench from the VBS phase to the FM phase, a straightforward correspondence between the behavior of the QSE and the DQPT can be observed. Specifically, the QSE changes successively from an origin-centered sphere to a prolate ellipsoid, and then to a needle at the critical dynamical time. However, the situation is much more complicated for the quench in the opposite direction as the QSE exhibits rather complex behavior. At last, we have also explored the change of the quantum correlations during the time evolution, which provides a more physical understanding of the QSE picture. Our findings indicate that the QSE concept can reveal the DQPTs in the 1D DQCP model from a geometric standpoint, which is impossible with conventional approaches.

The rest of the paper is organized as follows. In Sec. II, we first present a formal description of the model under study, and give a concise review of the QSE framework. The numerical findings and relevant discussions are then exhibited in Sec. III. Finally, the main results are summarized with a conclusion in Sec. IV.

II. THEORETICAL FRAMEWORK

A. Quantum steering ellipsoid

Before the discussion of our main results, it is helpful to describe the QSE framework [51] briefly here. Generally, any two-qubit quantum state ρ shared by Alice and Bob can be expanded in the Pauli basis as

$$\rho = \frac{1}{4} \sum_{\mu, \nu=0}^3 \Theta_{\mu\nu} \sigma^\mu \otimes \sigma^\nu, \quad (2)$$

with $\Theta_{\mu\nu} = \text{Tr}[\rho(\sigma^\mu \otimes \sigma^\nu)]$, σ^0 the 2×2 identity matrix, and $\sigma^{\mu, \nu \neq 0}$ standard Pauli matrices. The matrix Θ can be divided into a block form

$$\Theta = \begin{pmatrix} 1 & \mathbf{b}^T \\ \mathbf{a} & T \end{pmatrix}, \quad (3)$$

where \mathbf{a} and \mathbf{b} are Bloch vectors of the reduced states of Alice and Bob, respectively; T is the corresponding correlation matrix. By performing a positive operator valued measure

(POVM) on Bob's qubit, one can "steer" Alice's qubit to an appropriate state, named the steered state (see Appendix A). Considering all potential local measurements performed by Bob, the set of Alice's steered states $\{\mathbf{a}\}$ then constitutes Alice's QSE in the 3D Euclidean space, denoted by \mathcal{E}_A , centered at

$$\mathbf{c} = \frac{\mathbf{a} - T\mathbf{b}}{1 - b^2}. \quad (4)$$

The orientation and the lengths of Alice's steering ellipsoid semiaxes $s_i = \sqrt{q_i}$ are given by the eigenvectors \mathbf{v}_i and eigenvalues q_i of the ellipsoid matrix (I is the 3×3 identity matrix)

$$Q = \left(\frac{T - \mathbf{a}\mathbf{b}^T}{1 - b^2} \right) \left(I + \frac{\mathbf{b}\mathbf{b}^T}{1 - b^2} \right) (T^T - \mathbf{b}\mathbf{a}^T). \quad (5)$$

In general, Alice's QSE \mathcal{E}_A and Bob's QSE \mathcal{E}_B are not identical. To obtain \mathcal{E}_B , we just replace \mathbf{a} with \mathbf{b} , \mathbf{b} with \mathbf{a} , and T with T^T in Eq. (4) and Eq. (5). The geometric data $(\mathcal{E}_A, \mathbf{a}, \mathbf{b})$, where $\mathcal{E}_A = (\mathbf{c}, Q)$, provide a faithful representation of two-qubit quantum states. Besides, the volume of the steering ellipsoid is a fundamental property that captures a substantial fraction of nontrivial quantum correlations [51]. The volume of Alice's QSE can be calculated by

$$V = \frac{64\pi}{3} \frac{|\det \rho - \det \rho^{T_B}|}{(1 - b^2)^2}, \quad (6)$$

where b is the norm of the Bloch vector \mathbf{b} , and ρ^{T_B} denotes the partial transpose of the quantum state ρ with respect to Bob. Since the steering ellipsoid is constrained to lie within the Bloch sphere, its volume value can never exceed $V_{\max} = 4\pi/3$. The upper bound is achieved if and only if Alice and Bob share a pure entangled two-qubit state [51]; the steering ellipsoids of such states coincide with the Bloch sphere.

The fundamental advantage of the QSE is that both the intensity and type of quantum correlations can be reflected in related geometric properties, such as the shape and volume of the steering ellipsoid, which are independent of the reference-basis choice. Here, we mention some specific connections between the QSE and quantum correlations. It has established that a state is separable if it obeys a "nested tetrahedron" condition [51]. As a generalization of the Bloch sphere for single-qubit states to the description of two-qubit states, QSE has also been used to study the geometric representation of entanglement witness [55].

Inspired by these pioneering works, in this paper, we aim to explore the possibility of visualizing DQPTs by making use of the QSE. Furthermore, the dynamical behaviors of other relevant quantum information concepts, such as quantum entanglement and quantum coherence, are also examined similarly; this can be a valuable supplement to the QSE picture.

Here, we adopt the concurrence as the measure of two-qubit entanglement [62],

$$E_C(\rho_{i,i+1}) = \max\{0, \sqrt{\lambda_1} - \sqrt{\lambda_2} - \sqrt{\lambda_3} - \sqrt{\lambda_4}\}, \quad (7)$$

where λ_m denote the eigenvalues of $\rho_{i,i+1} \tilde{\rho}_{i,i+1}$ arranged in descending order with $\tilde{\rho}_{i,i+1} = (\sigma_i^y \otimes \sigma_{i+1}^y) \rho_{i,i+1}^* (\sigma_i^y \otimes \sigma_{i+1}^y)$ the time-reversed density matrix. Since the concurrence is ap-

plied on two lattice sites, it can only unveil the local structure of the entanglement stored in the system. In contrast, multipartite entanglement gives a more comprehensive description of the entanglement distribution across different parties of the system and, therefore, merits additional investigation [59]. Based on a general monogamy inequality obeyed by the entanglement of formation E_f for an arbitrary N -qubit state, a computable measure of the multipartite entanglement, named residual entanglement, can be defined accordingly by [63]

$$\tau \equiv E_f^2(\rho_{A_1|A_2\dots A_N}) - \sum_{i \neq 1}^N E_f^2(\rho_{A_1 A_i}), \quad (8)$$

where $E_f(\rho_{A_1|A_2\dots A_N})$ represents the entanglement in the partition $A_1|A_2\dots A_N$, and $E_f(\rho_{A_1 A_i})$ quantifies the one in the bipartite system $A_1 A_i$. The residual entanglement τ can be understood as the quantum entanglement that is not stored in spin pairs. In general, the calculation of τ relies on the specific choice of a target site, e.g., the A_1 in Eq. (8). In our case, however, this choice is unimportant due to the translation and parity symmetries. While QSE can be extended to multiqubit cases [51,64], it is noted that residual entanglement bears no direct connection to the QSE used in our work (which is defined for two-qubit states); therefore, τ can behave very differently from the above quantities and deserves an independent exploration.

Finally, as another key concept in quantum mechanics, quantum coherence has been considered a vital resource in quantum communication [65]. In some cases, quantum coherence could be a faithful diagnostic for equilibrium quantum phase transitions [66–68]. Here, we specifically use the l_1 -norm coherence [69] (in a fixed reference basis),

$$C_{l_1}(\rho) = \sum_{i \neq j} |\rho_{ij}|, \quad (9)$$

which is just the sum of the off-diagonal element magnitudes of the density matrix, to aid the understanding of our QSE results.

B. One-dimensional spin-1/2 model with deconfined critical point

In the present work, we consider the recently proposed 1D incarnation of DQCP in a spin-1/2 chain described by the Hamiltonian [41,42]

$$H = \sum_{i=1}^N (-J_x \sigma_i^x \sigma_{i+1}^x - J_z \sigma_i^z \sigma_{i+1}^z + K_x \sigma_i^x \sigma_{i+2}^x + K_z \sigma_i^z \sigma_{i+2}^z), \quad (10)$$

with σ_i^α ($\alpha = x, z$) the Pauli matrices on the i th lattice site and N the chain length; $J_x \geq 0$, $J_z \geq 0$, and $K_x \geq 0$, $K_z \geq 0$ are coupling constants for nearest and next-nearest neighbors, respectively. With fixed parameters $J_x = 1$ and $K_x = K_z = 1/2$, the system undergoes a phase transition from a VBS dimerized phase breaking the translation symmetry to another FM phase breaking the \mathbb{Z}_2 on-site symmetry by increasing J_z through the critical point $J_z^c \approx 1.465$. Existing large-scale simulation works have supported this phase transition to be

an analog of the DQCP in 1D case by performing conventional finite-size scaling analyzes [42,43,45]. While the static aspects of this DQCP model have brought fruitful results, its relevant dynamical behaviors have also shown many interesting physics [46,50,70], one of which is the possibility of supporting DQPTs between two quantum phases breaking very different symmetries [50]. By adopting the QSE approach, we aim to provide a different perspective for the DQPTs realized in this DQCP model; a general discussion about the relationship between the QSE and DQPT is, however, beyond the scope of this paper and needs future studies.

Unless otherwise specified, the quench process is carried out by rapidly adjusting the nearest-neighbor coupling J_z from an initial value J_z^{ini} to another final value J_z^{fin} with fixed Hamiltonian parameters $K_x = K_z = 1/2$ and $J_x = 1$. The time evolution driven by the quench Hamiltonian $H(J_z^{\text{fin}})$ is performed by the GSE-TDVP algorithm [61], which shows slower bond-dimension growth compared with the conventional TDVP [71,72] (also see Appendix B). In the MPS framework, the time-evolved quantum state $|\psi(t)\rangle$ will be described as

$$|\psi(t)\rangle = \sum_{\sigma} \text{Tr}(A_1^{\sigma_1} \cdots A_N^{\sigma_N}) |\sigma_1, \dots, \sigma_N\rangle, \quad (11)$$

where $A_i^{\sigma_i}$ are matrices with appropriate bond dimensions (the explicit time-dependence of A matrices are omitted here for simplicity). For the results shown in this work, the QSE method will be applied on one of the dimerized bonds of the 1D DQCP model (in the VBS region). To obtain the two-qubit reduced density matrix associated with the dimerized bond $(i, i+1)$ appearing in the QSE calculation, we trace out the qubits other than the i th and $(i+1)$ th qubits by

$$\rho_{i,i+1} = \sum_{\sigma} \sum_{\sigma'} \left[\text{Tr}(A_1^{\sigma_1} \cdots A_N^{\sigma_N}) \text{Tr}(A_1^{\sigma'_1} \cdots A_N^{\sigma'_N})^\dagger \times \prod_{k \neq i, i+1} \delta_{\sigma_k \sigma'_k} \right] |\sigma_i, \sigma_{i+1}\rangle \langle \sigma'_i, \sigma'_{i+1}|. \quad (12)$$

The convergence of the algorithm is examined in Appendix C; the relevant parameters concerning the simulation are also given therein. The calculations are mainly implemented by using the ITensor Library [73] with periodic boundary conditions.

III. NUMERICAL RESULTS AND DISCUSSION

In this section, the DQPT supported in the 1D DQCP chain will be explored with the QSE concept. In a previous work [50], it was observed that the DQCP model (10) can exhibit DQPTs for quenches from a VBS state to a FM state and vice versa. While the Loschmidt rate $\lambda(t)$ and dynamical order parameters $D(t)$ have provided convincing evidence for the existence of DQPTs, there are still some remaining questions. First, in Ref. [50], it established an exact mapping between the quench from the Majumdar-Ghosh (MG) state [74,75] to the FM state in the DQCP chain and the one from the paramagnetic state to the classical Ising state in the quantum transverse-field Ising model by considering $\lambda(t)$ and $D(t)$. This means that we cannot efficiently distinguish these two

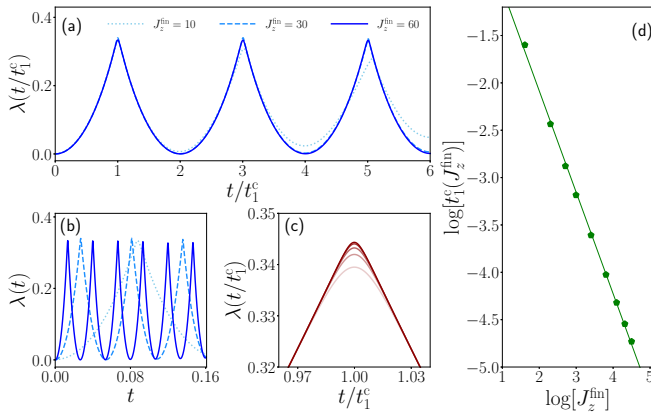


FIG. 1. The time dependence of (a) the rescaled Loschmidt rate function $\lambda(t/t_1^c)$ and (b) the rate function $\lambda(t)$ for the quench from $J_z^{\text{ini}} = 1$ to $J_z^{\text{fin}} = 10, 30, 60$ with $N = 96$. (c) The rescaled rate function $\lambda(t/t_1^c)$ of different system sizes $N = 528, 480, 384, 288, 192$ from top to bottom for the quench ending up with $J_z^{\text{fin}}/J_x = 300 \gg 1$. (d) Power-law scaling of the first critical time $t_1^c(J_z^{\text{fin}})$ with respect to J_z^{fin} .

cases by simply monitoring $\lambda(t)$ and $D(t)$. Second, the choice of the dynamical order parameter depends on the problem under study and requires prior knowledge about the initial state. This approach will meet difficulties when the definition of the dynamical order parameter is ambiguous. We will address these issues with the QSE concept in the following.

A. Quench from the VBS phase to the FM phase

First, we investigate the quench of the DQCP chain (10) from the VBS phase to the FM phase. For the sake of simplicity, we set the initial state to be the MG state ($J_z^{\text{ini}} = 1$) and then study the quench dynamics of different J_z^{fin} . The simulation results of the Loschmidt rate function $\lambda(t)$ are shown in Fig. 1(b). It is found that $\lambda(t)$ exhibits periodic peaks during the time evolution; the nonanalyticities in the form of kinks indicate the occurrence of DQPTs at critical times $t_n^c = t_1^c(2n + 1)$ with t_1^c the position of the first peak [see Fig. 1(c)]. Differently from the analytical calculations performed in Ref. [50] by ignoring J_x , K_x , and K_z terms, our numerical simulations have retained these omitted terms. This difference can be unveiled by graphing $\lambda(t/t_1^c)$ of different J_z^{fin}

in one plot. It is obvious from Fig. 1(a) that the rescaled critical time t_n^c/t_1^c deviates gradually from the prediction $(2n + 1)$ made in Ref. [50] as the decrease of J_z^{fin} . Despite this imperfection, the first occurrence of the DQPT seems insensitive to J_z^{fin} as an excellent data collapse can be achieved for the time range $t/t_1^c \in [0, 2]$. Furthermore, the first critical time t_1^c shows a power-law behavior with respect to J_z^{fin} , which is characterized by an exponent α . From an algebraic fit to $t_1^c(J_z^{\text{fin}}) \sim [J_z^{\text{fin}}]^{-\alpha}$ in Fig. 1(d), we find $\alpha = 1.070(4)$ compatible with the relation $t_1^c \propto 1/J_z^{\text{fin}}$ derived in Ref. [50]. Our findings are consistent with previous results and confirm the existence of DQPTs for the quench from the VBS phase to the FM phase.

Having explored the DQPT using the conventional approach, $\lambda(t)$, we now illustrate how the QSE can reveal DQPTs in a geometric way. For the VBS-to-FM quench, the initial state is set to the MG state ($\{|\uparrow\rangle_i, |\downarrow\rangle_i\}$ is the eigenbasis of the Pauli operator σ_i^z) [74,75]

$$|D\rangle = \bigotimes_{m=1}^{N/2} \frac{|\uparrow\rangle_{2m-1} |\uparrow\rangle_{2m} + |\downarrow\rangle_{2m-1} |\downarrow\rangle_{2m}}{\sqrt{2}}. \quad (13)$$

The fundamental strategy is then to indicate the DQPT through changes in the form and volume of the QSE during the time evolution.

As seen in Fig. 2, since the initially dimerized bond is one of the maximally entangled Bell states, the QSE at time $t/t_1^c = 0$ is an origin-centered sphere as expected, coinciding with the Bloch sphere. Here, the two-qubit state that enters the QSE method is associated with the central odd bond of the model. It is noted that the QSEs \mathcal{E}_{2m-1} and \mathcal{E}_{2m} associated, respectively, with the $(2m - 1)$ th and $2m$ th sites are identical during the time evolution due to the parity symmetry of the model (10) and the MG state (13). Hereafter, the subscript will be omitted if not necessary. As the quench continues into the region $0 < t/t_1^c < 1$, \mathcal{E} begins to shrink, but the vertical axis stays unchanged, leading to a radially aligned ellipsoid. Specifically, the QSE at the critical time has the form of a needle distinguishing itself from other states. After evolving beyond the critical time, the needle-shaped ellipsoid goes through the prolate ellipsoid back to a sphere. Consequently, we can obtain a clear correspondence between the QSE form and the VBS-to-FM DQPT; it suggests that the QSE is a powerful visualization tool for general quench dynamics.

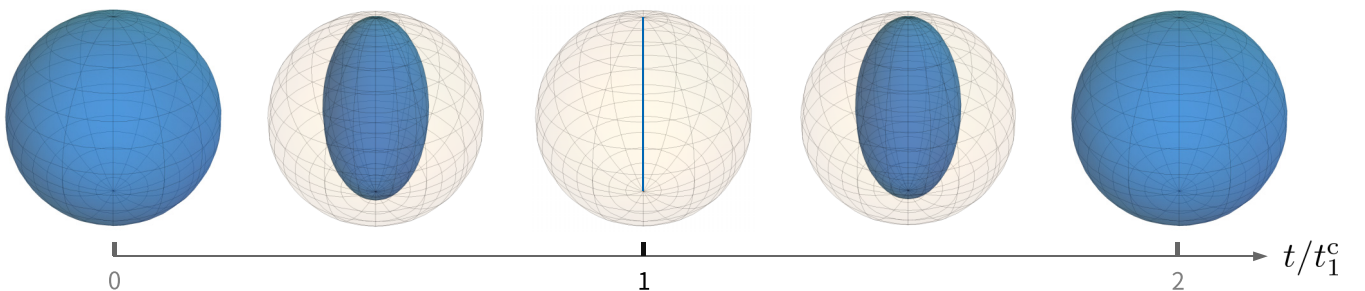


FIG. 2. The time evolution of the QSE for the quench from $J_z^{\text{ini}} = 1$ to $J_z^{\text{fin}} = 300$ in the 1D DQCP model. As depicted, the QSE changes from an origin-centered sphere at $t/t_1^c = 0$ to an ever-shrinking radially aligned ellipsoid within $0 < t/t_1^c < 1$, and then to a needle at the first critical time $t/t_1^c = 1$. Here, the orientation and the lengths of ellipsoid semiaxes are given by the eigenvectors and eigenvalues of the ellipsoid matrix (5). The system size is $N = 96$.

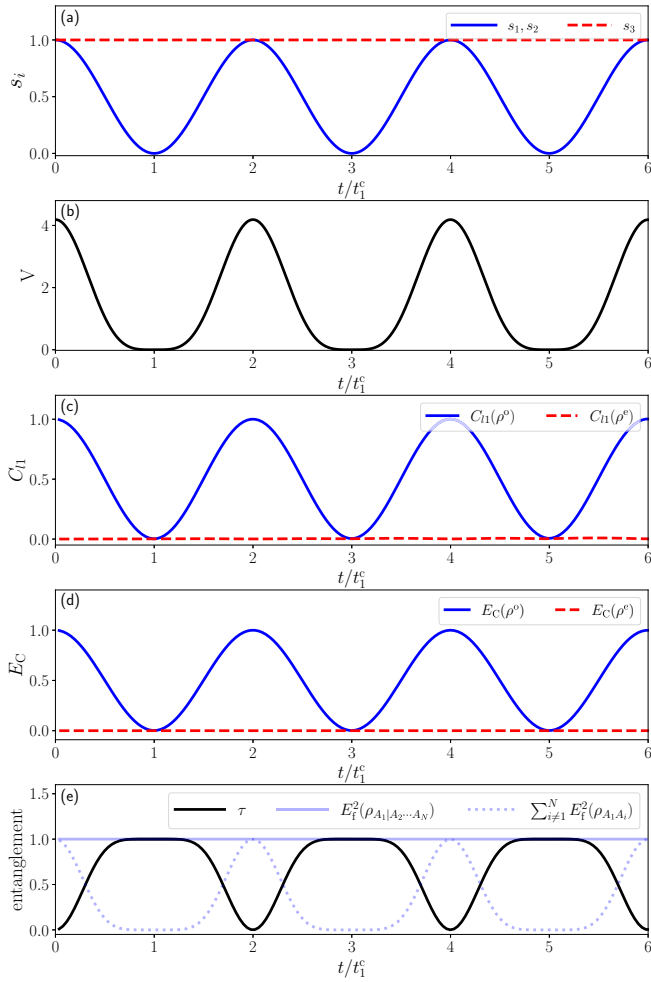


FIG. 3. Time evolution of the quantities defined in Sec. II, including (a) three semiaxes $s_{i=1,2,3}$, (b) the volume V of the QSE, (c) the quantum coherence C_{l_1} , (d) the concurrence E_C on the odd and even bonds, and (e) the residual entanglement τ , for the VBS-to-FM quench in the DQCP model (10). The relevant parameters set here are the same as in Fig. 2.

To provide a more quantitative perspective for the DQPT and help the understanding of the QSE picture, we also calculate the time evolution of the quantities defined in Sec. II. First, we focus on the quantities related directly to the QSE, i.e., its semiaxes s_i and volume value V . It is evident from Figs. 3(a) and 3(b) that the semiaxes s_1, s_2 and the volume V display periodic behaviors consistent with the QSE picture in Fig. 2; the vanishing points of s_1, s_2 and V can estimate the DQPT critical times since the QSE is a radial line there.

Further motivated by the connection between the QSE and other quantum information concepts (see Sec. II), we additionally calculate the concurrence E_C , the coherence C_{l_1} , and the residual entanglement τ in Figs. 3(c), 3(d), and 3(e), respectively. Note that all the quantities are computed with the reference basis $\{|\uparrow\rangle, |\downarrow\rangle\}^{\otimes N}$. It is observed that the bipartite entanglement and coherence of the odd bond $(2m-1, 2m)$ both reach their maximum exactly as the volume reaches its maximum, while τ is close to zero. The results indicate that the entanglement of the initial state is mainly stored in

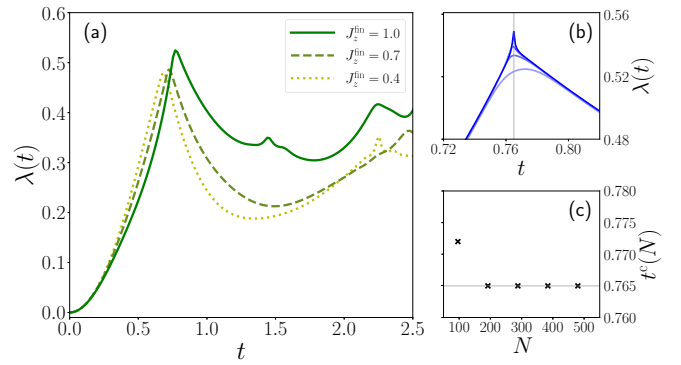


FIG. 4. (a) DQPTs in the Loschmidt rate function $\lambda(t)$ for the quench from the FM state to the VBS state of $J_z^{\text{fin}} = 1.0, 0.7, 0.4$. Here, the chain length is 96. (b) Loschmidt rate function $\lambda(t)$ in the vicinity of the critical time for the quench ending up with $J_z^{\text{fin}} = 1$. The results are shown for system sizes $N = 96, 192, 288, 384$ from bottom to top. (c) The rapid convergence of the finite-size critical time [determined by the local maximum of $\lambda(t)$ in (b)] with respect to N .

odd bonds, i.e., dimers in the MG state (13). It is interesting that, as time increases, the entanglement of the even bond $(2m, 2m+1)$ remains at zero, implying the robustness of the VBS dimer pattern throughout the quench process. Moreover, there is a periodic change in the entanglement distribution during the time evolution. To clarify this observation, we display the results of the two terms on the right-hand side of Eq. (8) in Fig. 3(e) separately. As the critical time is approached, the entanglement stored in spin pairs, which is characterized by $\sum_{i \neq 1} E_i^2(\rho_{A_1 A_i})$, transfers gradually to entanglement shared by at least three sites (the increase of τ). It suggests that the quench dynamics in the 1D DQCP chain can be a natural candidate for entanglement switches.

Using the QSE concept, we have unveiled the DQPT for the VBS-to-FM quench in the 1D DQCP chain. Now we can explain how the QSE can address the issues raised at the beginning of the section. First, in our paper, the application of the QSE concept on two nearest-neighbor sites is quite simple and requires no prior knowledge of the initial state or the quench Hamiltonian. Therefore, the QSE can be a convenient tool in the study of other DQPTs. Second, as shown in Ref. [50], there is an exact mapping between the quench from the MG state to the FM state in the DQCP model and the one from the paramagnetic state to the classical Ising state in the transverse field Ising chain, and the Loschmidt rate function cannot efficiently distinguish these two cases. This task can be accomplished by employing the QSE concept. As the two nearest-neighbor sites in the paramagnetic state are just a product state, the evolution of the QSE will start from a single point on the Bloch sphere, which is distinct from the case in Fig. 2.

B. Quench from the FM phase to the VBS phase

We shall finally present the results for the quench from one of the doubly degenerate FM states to the VBS state. Figure 4(a) shows the time dependence of $\lambda(t)$ for quenches that end up with $J_z^{\text{fin}} = 1.0, 0.7, 0.4$. In contrast to the VBS-

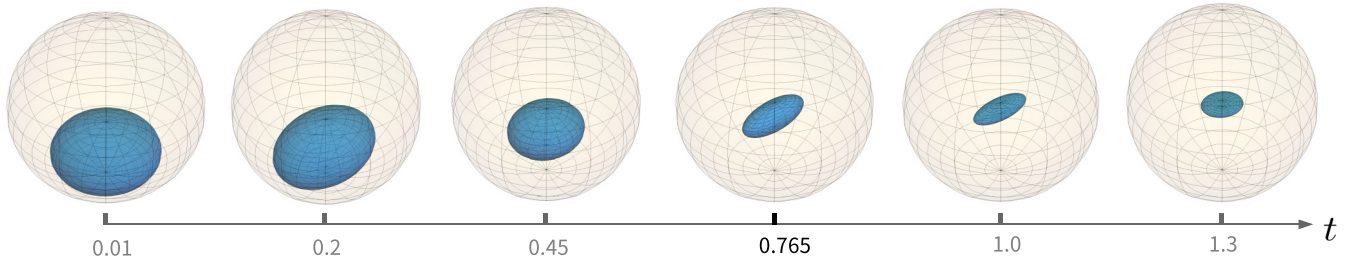


FIG. 5. The time evolution of the QSE for the quench from the FM state (polarized along the negative z axis) to the MG state in the 1D DQCP chain. Since the initial state at $t = 0$ is a product state with $b = 1$, the corresponding \mathcal{E} consists of a single point on the Bloch sphere. Therefore, the dynamic of the QSE is drawn from the pseudoinitial state at $t = 0.01$ with $b \neq 1$. Here, the orientation and the lengths of ellipsoid semiaxes are given by the eigenvectors and eigenvalues of the ellipsoid matrix (5). The critical time $t^c = 0.765$ is obtained from Fig. 4(c).

to-FM quench discussed earlier, the time evolution of the Loschmidt rate function is nonperiodic here. However, we can still observe a nonanalytic structure of $\lambda(t)$ in a short timescale [see Fig. 4(b)], supporting the existence of a DQPT during the time evolution. For the sake of simplicity, hereafter, we will only focus on the case of $J_z^{\text{fin}} = 1$. Figure 4(c) shows the finite-size effect of the critical time as a function of the chain length. It is clear that the pseudocritical time converges to its true value very fast, and the chain of length 200 can represent the thermodynamic limit faithfully. Here we have provided a more detailed study of the Loschmidt rate function compared with previous work [50], especially the convergence of the critical time and the robustness of the DQPT for different J_z^{fin} .

In Fig. 5, we continue to investigate the dynamics of the QSE to unveil more aspects of the DQPT. The illustration of the dynamical shape of the QSE is associated with the central odd bond. Note that Eqs. (4), (5), and (6) are well defined only if $b \neq 1$; for the initial state $|\psi(0)\rangle = \bigotimes_{i=1}^N |\downarrow\rangle_i$, however, we find that $b = 1$, and \mathcal{E} consists of a single point sitting on the Bloch sphere. Therefore, steering ellipsoids are only drawn

for $t > 0$ in Fig. 5. Following the quench evolution, more complicated steering ellipsoid dynamics emerge, as shown explicitly in Figs. 5 and 6. At the same time, the volume of the steering ellipsoid decreases monotonically with increasing time [Fig. 6(a)], implying the loss of the quantum correlation; the semiaxes s_i display a rather complex behavior featured by avoided crossings [Fig. 6(b)]. The crossings provide a reliable indication for the abrupt change of the ellipsoid orientation (the direction along the longest semiaxis) during the time evolution. Moreover, there may be a relationship between the DQPT and the crossing of the shortest two semiaxes from Fig. 6(b) since the DQPT happens just after the crossing. Similar observations have also been made for the case of $J_z^{\text{fin}} = 0.7$ and 0.4 (the data are not displayed here); however, the underlying connection is still unclear and requires future studies. In Fig. 6(c), we finally plot the distance of the ellipsoid center from the origin $|\mathbf{c}|$, which decays very quickly to a small value, implying that the QSE will eventually stay in the vicinity of the origin.

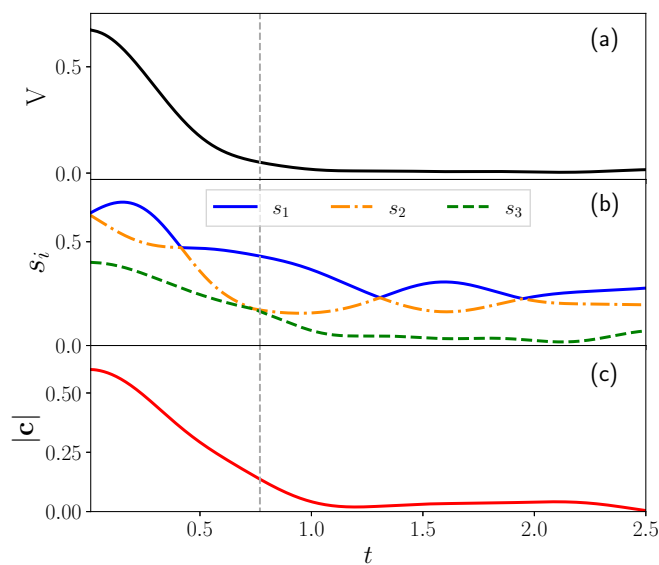


FIG. 6. (a) The volume V , (b) the semiaxes s_i of the QSE, and (c) the distance of the ellipsoid center from the origin $|\mathbf{c}|$ for the FM-to-MG quench. The vertical dashed line indicates the critical time t^c . The relevant parameters set here are the same as in Fig. 5.

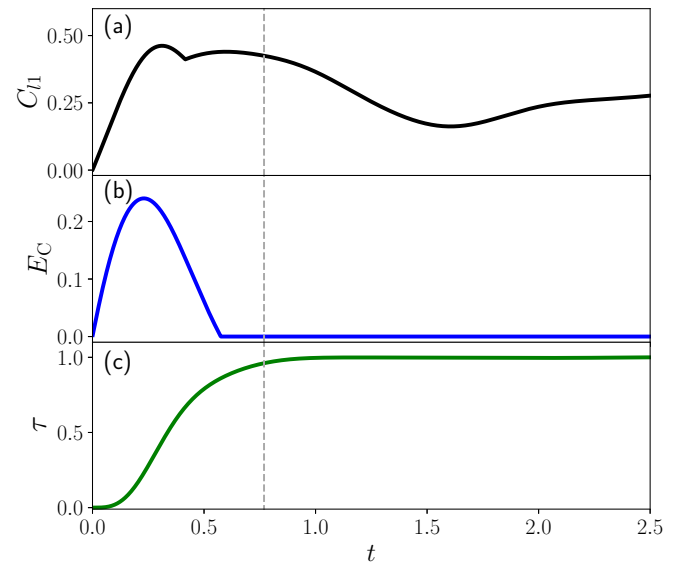


FIG. 7. The dynamics of (a) the quantum coherence C_{l_1} , (b) the concurrence E_C , and (c) the residual entanglement τ in the 1D DQCP chain for the FM-to-MG quench. The vertical gray dashed line indicates the critical time t^c . The relevant parameters set here are the same as in Fig. 5.

As before, now, we turn to examine the evolution of the quantum correlations in the quench dynamics. It is found from Figs. 7(a) and 7(b) that the quantum coherence C_{l_1} and concurrence E_C both experience rapid growth at the early stage of the FM-to-VBS quench and reach the maximums separately. This observation seems to conflict with the monotonically decreasing of the ellipsoid volume V [Fig. 6(a)]. We note, however, that there are three geometric contributions to the correlations between qubits [51]: the distance $|c|$, the volume V , and the alignment of the ellipsoid relative to the radial direction. While the volume indicates a loss of the correlation, the involvement of the latter two contributions can still support an enhancement of the correlations. As time increases, the volume contribution becomes dominant; the concurrence drops quickly to the zero value, and the coherence decays slowly to an equilibrium value with an oscillatory behavior. The results give a more physical understanding of the QSE picture illustrated in Fig. 5. At last, as shown in Fig. 7(c), the residual entanglement τ shows a monotonic growth before attaining a plateau near the DQPT. Although the quantities explored here cannot determine the critical time of the DQPT, they give additional insight into the underlying physical mechanisms in the vicinity of the DQPT under study.

IV. CONCLUSION

In this work, intending to unveil how the QSE concept can characterize the DQPTs, we focused on the quench dynamics in a 1D spin chain with a DQCP. Assisted by the recently developed GSE-TDVP algorithm, this goal has been refined to study the relationship between the geometric properties of the QSE and the quench crossing the deconfined critical point in the present model. Moreover, different measures of quantum correlations, i.e., the concurrence, the l_1 -norm coherence, and the residual entanglement, were also examined to supplement the QSE picture. It has demonstrated that the QSE can efficiently capture the DQPTs and determine the critical dynamical time when the system is quenched from the MG state to the FM state. As depicted in the main text, the QSE changes from a Bloch sphere to a prolate ellipsoid, particularly at the critical dynamical time, to a needle distinguishing itself from other states. For the quench from the FM state to the MG state, however, the QSE exhibits a more complicated behavior. While the connection between the QSE and the DQPT is unclear in this situation, together with the computed measures of quantum correlations, the results still uncover some underlying physics near the DQPT. These

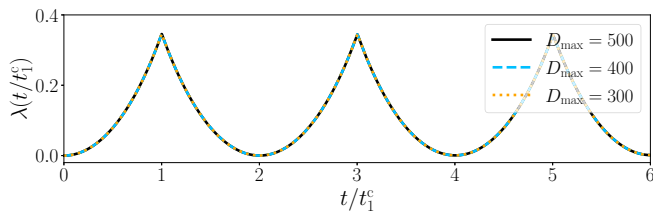


FIG. 8. The convergence of the GSE-TDVP simulation with respect to the MPS bond dimension D_{\max} by observing the Loschmidt rate function $\lambda(t)$ in the quench dynamics ($J_z^{\text{ini}} = 1 \rightarrow J_z^{\text{fin}} = 60$). Here, the time step is 10^{-5} and the chain length is 528.

findings indicate that the QSE concept can reveal DQPTs and associated quantum correlations of the present model in a geometrically discernible manner.

As the application of the QSE relies on no prior knowledge of the initial state or the model under study, we anticipate that the QSE can provide a convenient tool for the visualization of general nonequilibrium quantum many-body dynamics such as many-body localization [76] or quantum time crystals [77]. Our work also provides some insight into the nonequilibrium experiments using QSE. Given that DQPTs are assumed to occur at absolute-zero temperatures, which are difficult to accomplish experimentally, there may be a discrepancy between theory and experiment regarding the detection of DQPTs. Fortunately, the validation of QSE was illustrated experimentally [60]. Thus, we can expect that revealing DQPTs through QSE established here could be verified experimentally in the near future.

ACKNOWLEDGMENTS

The numerical calculations were run on the Kirin No. 2 High Performance Cluster supported by the Institute for Fusion Theory and Simulation (IFTS) at Zhejiang University. This work was supported by the National Natural Science Foundation of China under Grant No. 11975198.

APPENDIX A: CONSTRUCTION OF QSE

We provide here further details about the construction of the steering ellipsoid. First, we express POVM elements in the Hilbert-Schmidt space. When Bob does a measurement on his qubit, each measurement outcome can be associated with a POVM element $\mathcal{M} = \{M\}$ with $M \geq 0$. Generally, M can be assigned to a Hermitian operator and thus can be written as $M = \sum_{\mu=0}^3 X_{\mu} \sigma^{\mu}$, where $X_{\mu} = \text{Tr}(M \sigma^{\mu})$ are components of the real four-component vector in row form $\mathbf{X} = (1, \mathbf{X}_k)$ with $\mathbf{X}_k = (X_1, X_2, X_3)$. The post-measurement state of Alice is steered to $\rho^A = \text{Tr}_B[\rho^{AB}(\mathbb{I} \otimes M)]$. Direct calculation shows that, combined with Eqs. (2) and (3), ρ^A can be given in the four-vector formalism as $\frac{1}{2} \Theta \mathbf{X}$ with probability $\frac{1}{2}(1 + \mathbf{b} \cdot \mathbf{X}_k^T)$. Taking into account all possible local measurements by Bob, the set of Alice's steered states can be geometrically represented by the set of Bloch vectors [51]

$$\mathcal{E}_A = \left\{ \frac{\mathbf{a} + T \mathbf{X}_k}{1 + \mathbf{b} \cdot \mathbf{X}_k} : |\mathbf{X}_k| \leq 1 \right\}, \quad (\text{A1})$$

which can be proven to form an ellipsoid in the 3D Euclidean space. The ellipsoid given by (A1) is the so-called ‘‘steering ellipsoid.’’

Next, as an example of the procedure, we outline in more detail how to construct a specific QSE. Consider a two-qubit system in a pure state [78]

$$|\psi^{AB}\rangle = \frac{1}{\sqrt{2}}(|\psi_0\rangle_A |\downarrow\rangle_B + |\psi_1\rangle_A |\uparrow\rangle_B), \quad (\text{A2})$$

where $|\psi_0\rangle_A = (|\downarrow\rangle + |\uparrow\rangle)/\sqrt{2}$ and $|\psi_1\rangle_A = 4/5|\downarrow\rangle + 3/5|\uparrow\rangle$. Let qubit A pass through a quantum channel with

Kraus operators

$$A_1 = |\downarrow\rangle\langle\downarrow| + \frac{1}{\sqrt{2}}|\uparrow\rangle\langle\uparrow|, \quad A_2 = \frac{1}{\sqrt{2}}|\downarrow\rangle\langle\uparrow|. \quad (\text{A3})$$

The output state of the channel is described by

$$\begin{aligned} \rho^{\text{AB}} &= \sum_{i=1}^2 (A_i \otimes \mathbb{I}) |\psi^{\text{AB}}\rangle \langle\psi^{\text{AB}}| (A_i \otimes \mathbb{I})^\dagger \\ &= \begin{pmatrix} \frac{3}{8} & \frac{11}{20\sqrt{2}} & \frac{1}{4\sqrt{2}} & \frac{3}{20} \\ \frac{11}{20\sqrt{2}} & \frac{41}{100} & \frac{1}{5} & \frac{3\sqrt{2}}{25} \\ \frac{1}{4\sqrt{2}} & \frac{1}{5} & \frac{1}{8} & \frac{3}{20\sqrt{2}} \\ \frac{3}{20} & \frac{3\sqrt{2}}{25} & \frac{3}{20\sqrt{2}} & \frac{9}{100} \end{pmatrix}. \end{aligned} \quad (\text{A4})$$

Then the Bloch vectors \mathbf{a} , \mathbf{b} , and correlation matrix T can be given by

$$\begin{aligned} \mathbf{a} &= \text{Tr}(\rho^{\text{AB}} \cdot \boldsymbol{\sigma} \otimes \mathbb{I}) = \left(\frac{49}{50\sqrt{2}}, 0, \frac{57}{100} \right)^T, \\ \mathbf{b} &= \text{Tr}(\rho^{\text{AB}} \cdot \mathbb{I} \otimes \boldsymbol{\sigma}) = \left(\frac{7}{5\sqrt{2}}, 0, 0 \right)^T, \\ T &= \text{Tr}(\rho^{\text{AB}} \cdot \boldsymbol{\sigma} \otimes \boldsymbol{\sigma}) = \begin{pmatrix} \frac{7}{10} & 0 & \frac{1}{50\sqrt{2}} \\ 0 & \frac{1}{10} & 0 \\ \frac{2\sqrt{2}}{5} & 0 & -\frac{7}{100} \end{pmatrix}. \end{aligned} \quad (\text{A5})$$

Substituting the above equations into Eq. (4), we find that the center of \mathcal{E}_A is at the point $\mathbf{c} = (0, 0, 1/2)^T$. From Eq. (5), we obtain the lengths of \mathcal{E}_A 's semiaxes $s_1^2 = s_2^2 = 1/2$, $s_3^2 = 1/4$, which are the eigenvalues of matrix Q . Under these conditions, the equation of the quantum steering ellipsoid \mathcal{E}_A in the coordinate frame (x, y, z) takes the form

$$2(x^2 + y^2) + 4\left(z - \frac{1}{2}\right)^2 = 1. \quad (\text{A6})$$

APPENDIX B: THE GSE-TDVP ALGORITHM

This Appendix briefly describes the GSE-TDVP algorithm used in our numerical simulation. Prior research has established that the TDVP method based on the Lie-Trotter decomposition of the tangent space projector [71,72] can sometimes fail due to the loss of the orthogonality or the formation of excessively highly entangled states [49]. These issues have recently been overcome by an improved scheme, i.e., the GSE-TDVP [61]. The essential modification is the enlargement of the tangent space before each time-evolution step using global Krylov vectors. Specifically, in the simulation performed in the main text, the basis set of the state $|\psi(t)\rangle$ at time t is extended first by the Krylov subspace of order k ,

$$\mathcal{K}_k(H, |\psi(t)\rangle) = \text{span}\{|\psi(t)\rangle, H|\psi(t)\rangle, \dots, H^{k-1}|\psi(t)\rangle\}, \quad (\text{B1})$$

before evolving to the time $t + \Delta t$. For a small time step Δt , by writing the time evolved state as

$$|\psi(t + \Delta t)\rangle = \exp(-iH\Delta t)|\psi(t)\rangle = \sum_{l=0}^{\infty} \frac{(-i\Delta t)^l}{l!} H^l |\psi(t)\rangle, \quad (\text{B2})$$

we can expect that a relatively small value of the order k in Eq. (B1) should be sufficient to efficiently represent the state $|\psi(t + \Delta t)\rangle$. In practice, the extension of the basis set is done by carrying out singular value decompositions with truncation error ϵ_M . Besides, when applying the matrix product operator H iteratively on $|\psi(t)\rangle$, we choose a suitable truncation cutoff ϵ_K and a maximum MPS bond dimension D_{max} to control the rapid growth of the bond dimension of $H^l|\psi(t)\rangle$. The full description and benchmark analysis of the algorithm can be found in Ref. [61].

APPENDIX C: CONVERGENCE OF THE GSE-TDVP RESULTS

In the main text, the GSE-TDVP simulation was implemented with the parameter setting $k = 3$, $\epsilon_M = 10^{-12}$, $\epsilon_K = 10^{-12}$, and $D_{\text{max}} = 500$. In Fig. 8, we show the convergence of the Loschmidt rate function $\lambda(t)$ with respect to D_{max} for the quench from $J_z^{\text{ini}} = 1$ to $J_z^{\text{fin}} = 60$ with time step $\Delta t = 10^{-5}$.

- [1] A. Browaeys and T. Lahaye, Many-body physics with individually controlled Rydberg atoms, *Nat. Phys.* **16**, 132 (2020).
 [2] S. Hart, H. Ren, T. Wagner, P. Leubner, M. Mühlbauer, C. Brüne, H. Buhmann, L. W. Molenkamp, and A. Yacoby, Induced superconductivity in the quantum spin Hall edge, *Nat. Phys.* **10**, 638 (2014).
 [3] M. Suda, R. Kato, and H. M. Yamamoto, Light-induced superconductivity using a photoactive electric double layer, *Science* **347**, 743 (2015).
 [4] M. Mitrano, A. Cantaluppi, D. Nicoletti, S. Kaiser, A. Perucchi, S. Lupi, P. D. Pietro, D. Pontiroli, M. Riccò, D. J. S. R. Clark, and A. Cavalleri, Possible light-induced superconductivity in K_3C_{60} at high temperature, *Nature (London)* **530**, 461 (2016).

- [5] J. Eisert, M. Friesdorf, and C. Gogolin, Quantum many-body systems out of equilibrium, *Rep. Prog. Phys.* **11**, 124 (2015).
 [6] M. Heyl, A. Polkovnikov, and S. Kehrein, Dynamical Quantum Phase Transitions in the Transverse-Field Ising Model, *Phys. Rev. Lett.* **110**, 135704 (2013).
 [7] M. Heyl, Dynamical quantum phase transitions: A review, *Rep. Prog. Phys.* **81**, 054001 (2018).
 [8] S. Vajna and B. Dóra, Disentangling dynamical phase transitions from equilibrium phase transitions, *Phys. Rev. B* **89**, 161105(R) (2014).
 [9] F. Andraschko and J. Sirker, Dynamical quantum phase transitions and the Loschmidt echo: A transfer matrix approach, *Phys. Rev. B* **89**, 125120 (2014).

- [10] M. Heyl, Scaling and Universality at Dynamical Quantum Phase Transitions, *Phys. Rev. Lett.* **115**, 140602 (2015).
- [11] S. Sharma, S. Suzuki, and A. Dutta, Quenches and dynamical phase transitions in a nonintegrable quantum Ising model, *Phys. Rev. B* **92**, 104306 (2015).
- [12] C. Karrasch and D. Schuricht, Dynamical quantum phase transitions in the quantum Potts chain, *Phys. Rev. B* **95**, 075143 (2017).
- [13] E. Canovi, P. Werner, and M. Eckstein, First-Order Dynamical Phase Transitions, *Phys. Rev. Lett.* **113**, 265702 (2014).
- [14] S. Vajna and B. Dóra, Topological classification of dynamical phase transitions, *Phys. Rev. B* **91**, 155127 (2015).
- [15] J. C. Halimeh and V. Zauner-Stauber, Dynamical phase diagram of quantum spin chains with long-range interactions, *Phys. Rev. B* **96**, 134427 (2017).
- [16] E. Canovi, E. Ercolessi, P. Naldesi, L. Taddia, and D. Vodola, Dynamics of entanglement entropy and entanglement spectrum crossing a quantum phase transition, *Phys. Rev. B* **89**, 104303 (2014).
- [17] G. Torlai, L. Tagliacozzo, and G. D. Chiara, Dynamics of the entanglement spectrum in spin chains, *J. Stat. Mech.* (2014) P06001.
- [18] S. De Nicola, A. A. Michailidis, and M. Serbyn, Entanglement View of Dynamical Quantum Phase Transitions, *Phys. Rev. Lett.* **126**, 040602 (2021).
- [19] J. C. Budich and M. Heyl, Dynamical topological order parameters far from equilibrium, *Phys. Rev. B* **93**, 085416 (2016).
- [20] S. Sharma, U. Divakaran, A. Polkovnikov, and A. Dutta, Slow quenches in a quantum Ising chain: Dynamical phase transitions and topology, *Phys. Rev. B* **93**, 144306 (2016).
- [21] M. Heyl and J. C. Budich, Dynamical topological quantum phase transitions for mixed states, *Phys. Rev. B* **96**, 180304(R) (2017).
- [22] U. Bhattacharya and A. Dutta, Emergent topology and dynamical quantum phase transitions in two-dimensional closed quantum systems, *Phys. Rev. B* **96**, 014302 (2017).
- [23] U. Bhattacharya, S. Bandyopadhyay, and A. Dutta, Mixed state dynamical quantum phase transitions, *Phys. Rev. B* **96**, 180303(R) (2017).
- [24] P. Jurcevic, H. Shen, P. Hauke, C. Maier, T. Brydges, C. Hempel, B. P. Lanyon, M. Heyl, R. Blatt, and C. F. Roos, Direct Observation of Dynamical Quantum Phase Transitions in an Interacting Many-Body System, *Phys. Rev. Lett.* **119**, 080501 (2017).
- [25] N. Fläschner, D. Vogel, M. Tarnowski, B. S. Rem, D. S. Luhmann, M. Heyl, J. C. Budich, Y. L. Mathe, K. Sengstock, and C. Weitenberg, Observation of dynamical vortices after quenches in a system with topology, *Nat. Phys.* **14**, 265 (2018).
- [26] T. Senthil, A. Vishwanath, L. Balents, S. Sachdev, and M. P. A. Fisher, Deconfined quantum critical points, *Science* **303**, 1490 (2004).
- [27] K. G. Wilson, The renormalization group: Critical phenomena and the Kondo problem, *Rev. Mod. Phys.* **47**, 773 (1975).
- [28] K. G. Wilson and J. Kogut, The renormalization group and the ϵ expansion, *Phys. Rep.* **12**, 75 (1974).
- [29] T. Senthil, L. Balents, S. Sachdev, A. Vishwanath, and M. P. A. Fisher, Quantum criticality beyond the Landau-Ginzburg-Wilson paradigm, *Phys. Rev. B* **70**, 144407 (2004).
- [30] A. W. Sandvik, Evidence for Deconfined Quantum Criticality in a Two-Dimensional Heisenberg Model with Four-Spin Interactions, *Phys. Rev. Lett.* **98**, 227202 (2007).
- [31] R. G. Melko and R. K. Kaul, Scaling in the Fan of an Unconventional Quantum Critical Point, *Phys. Rev. Lett.* **100**, 017203 (2008).
- [32] A. B. Kuklov, M. Matsumoto, N. V. Prokof'ev, B. V. Svistunov, and M. Troyer, Deconfined Criticality: Generic First-Order Transition in the SU(2) Symmetry Case, *Phys. Rev. Lett.* **101**, 050405 (2008).
- [33] A. W. Sandvik, Continuous Quantum Phase Transition between an Antiferromagnet and a Valence-Bond Solid in Two Dimensions: Evidence for Logarithmic Corrections to Scaling, *Phys. Rev. Lett.* **104**, 177201 (2010).
- [34] A. Banerjee, K. Damle, and F. Alet, Impurity spin texture at a deconfined quantum critical point, *Phys. Rev. B* **82**, 155139 (2010).
- [35] K. Chen, Y. Huang, Y. Deng, A. B. Kuklov, N. V. Prokof'ev, and B. V. Svistunov, Deconfined Criticality Flow in the Heisenberg Model with Ring-Exchange Interactions, *Phys. Rev. Lett.* **110**, 185701 (2013).
- [36] S. Pujari, K. Damle, and F. Alet, Néel-State to Valence-Bond-Solid Transition on the Honeycomb Lattice: Evidence for Deconfined Criticality, *Phys. Rev. Lett.* **111**, 087203 (2013).
- [37] H. Shao, W. Guo, and A. W. Sandvik, Quantum criticality with two length scales, *Science* **352**, 213 (2016).
- [38] X.-F. Zhang, Y.-C. He, S. Eggert, R. Moessner, and F. Pollmann, Continuous Easy-Plane Deconfined Phase Transition on the Kagome Lattice, *Phys. Rev. Lett.* **120**, 115702 (2018).
- [39] N. Ma, G.-Y. Sun, Y.-Z. You, C. Xu, A. Vishwanath, A. W. Sandvik, and Z. Y. Meng, Dynamical signature of fractionalization at a deconfined quantum critical point, *Phys. Rev. B* **98**, 174421 (2018).
- [40] J. Wildeboer, N. Desai, J. D'Emidio, and R. K. Kaul, First-order Néel to columnar valence bond solid transition in a model square-lattice $S = 1$ antiferromagnet, *Phys. Rev. B* **101**, 045111 (2020).
- [41] S. Jiang and O. Motrunich, Ising ferromagnet to valence bond solid transition in a one-dimensional spin chain: Analogies to deconfined quantum critical points, *Phys. Rev. B* **99**, 075103 (2019).
- [42] B. Roberts, S. Jiang, and O. I. Motrunich, Deconfined quantum critical point in one dimension, *Phys. Rev. B* **99**, 165143 (2019).
- [43] R.-Z. Huang, D.-C. Lu, Y.-Z. You, Z. Y. Meng, and T. Xiang, Emergent symmetry and conserved current at a one-dimensional incarnation of deconfined quantum critical point, *Phys. Rev. B* **100**, 125137 (2019).
- [44] Q. Luo, J. Zhao, and X. Wang, Intrinsic jump character of first-order quantum phase transitions, *Phys. Rev. B* **100**, 121111(R) (2019).
- [45] G. Sun, B.-B. Wei, and S.-P. Kou, Fidelity as a probe for a deconfined quantum critical point, *Phys. Rev. B* **100**, 064427 (2019).
- [46] N. Xi and R. Yu, Dynamical signatures of the one-dimensional deconfined quantum critical point, *Chin. Phys. B* **31**, 057501 (2022).
- [47] U. Schollwöck, The density-matrix renormalization group in the age of matrix product states, *Ann. Phys.* **326**, 96 (2011).

- [48] R. Orús, A practical introduction to tensor networks: Matrix product states and projected entangled pair states, *Ann. Phys.* **349**, 117 (2014).
- [49] S. Paeckel, T. Köhler, A. Swoboda, S. R. Manmana, U. Schollwöck, and C. Hubig, Time-evolution methods for matrix-product states, *Ann. Phys.* **411**, 167998 (2019).
- [50] G. Sun and B.-B. Wei, Dynamical quantum phase transitions in a spin chain with deconfined quantum critical points, *Phys. Rev. B* **102**, 094302 (2020).
- [51] S. Jevtic, M. Pusey, D. Jennings, and T. Rudolph, Quantum Steering Ellipsoids, *Phys. Rev. Lett.* **113**, 020402 (2014).
- [52] M. Shi, F. Jiang, C. Sun, and J. Du, Geometric picture of quantum discord for two-qubit quantum states, *New J. Phys.* **13**, 073016 (2011).
- [53] M. Shi, C. Sun, F. Jiang, X. Yan, and J. Du, Optimal measurement for quantum discord of two-qubit states, *Phys. Rev. A* **85**, 064104 (2012).
- [54] A. Milne, D. Jennings, S. Jevtic, and T. Rudolph, Quantum correlations of two-qubit states with one maximally mixed marginal, *Phys. Rev. A* **90**, 024302 (2014).
- [55] A. Milne, D. Jennings, and T. Rudolph, Geometric representation of two-qubit entanglement witnesses, *Phys. Rev. A* **92**, 012311 (2015).
- [56] S. Jevtic, M. J. W. Hall, M. R. Anderson, M. Zwierz, and H. M. Wiseman, Einstein-Podolsky-Rosen steering and the steering ellipsoid, *J. Opt. Soc. Am. B* **32**, A40 (2015).
- [57] H. C. Nguyen and T. Vu, Necessary and sufficient condition for steerability of two-qubit states by the geometry of steering outcomes, *Europhys. Lett.* **115**, 10003 (2016).
- [58] M.-M. Du, D.-J. Zhang, Z.-Y. Zhou, and D. M. Tong, Visualizing quantum phase transitions in the XXZ model via the quantum steering ellipsoid, *Phys. Rev. A* **104**, 012418 (2021).
- [59] L. Amico, R. Fazio, A. Osterloh, and V. Vedral, Entanglement in many-body systems, *Rev. Mod. Phys.* **80**, 517 (2008).
- [60] C. Zhang, S. Cheng, L. Li, Q.-Y. Liang, B.-H. Liu, Y.-F. Huang, C.-F. Li, G.-C. Guo, M. J. W. Hall, H. M. Wiseman, and G. J. Pryde, Experimental Validation of Quantum Steering Ellipsoids and Tests of Volume Monogamy Relations, *Phys. Rev. Lett.* **122**, 070402 (2019).
- [61] M. Yang and S. R. White, Time-dependent variational principle with ancillary Krylov subspace, *Phys. Rev. B* **102**, 094315 (2020).
- [62] W. K. Wootters, Entanglement of Formation of an Arbitrary State of Two Qubits, *Phys. Rev. Lett.* **80**, 2245 (1998).
- [63] Y.-K. Bai, Y.-F. Xu, and Z. D. Wang, General Monogamy Relation for the Entanglement of Formation in Multiqubit Systems, *Phys. Rev. Lett.* **113**, 100503 (2014).
- [64] A. Milne, S. Jevtic, D. Jennings, H. Wiseman, and T. Rudolph, Quantum steering ellipsoids, extremal physical states and monogamy, *New J. Phys.* **16**, 083017 (2014).
- [65] A. Streltsov, G. Adesso, and M. B. Plenio, Colloquium: Quantum coherence as a resource, *Rev. Mod. Phys.* **89**, 041003 (2017).
- [66] G. Karpat, B. Çakmak, and F. F. Fanchini, Quantum coherence and uncertainty in the anisotropic XY chain, *Phys. Rev. B* **90**, 104431 (2014).
- [67] Y.-C. Li and H.-Q. Lin, Quantum coherence and quantum phase transitions, *Sci. Rep.* **6**, 26365 (2016).
- [68] J.-J. Chen, J. Cui, Y.-R. Zhang, and H. Fan, Coherence susceptibility as a probe of quantum phase transitions, *Phys. Rev. A* **94**, 022112 (2016).
- [69] T. Baumgratz, M. Cramer, and M. B. Plenio, Quantifying Coherence, *Phys. Rev. Lett.* **113**, 140401 (2014).
- [70] R.-Z. Huang and S. Yin, Kibble-Zurek mechanism for a one-dimensional incarnation of a deconfined quantum critical point, *Phys. Rev. Res.* **2**, 023175 (2020).
- [71] J. Haegeman, J. I. Cirac, T. J. Osborne, I. Pižorn, H. Verschelde, and F. Verstraete, Time-Dependent Variational Principle for Quantum Lattices, *Phys. Rev. Lett.* **107**, 070601 (2011).
- [72] J. Haegeman, C. Lubich, I. Oseledets, B. Vandereycken, and F. Verstraete, Unifying time evolution and optimization with matrix product states, *Phys. Rev. B* **94**, 165116 (2016).
- [73] M. Fishman, S. R. White, and E. M. Stoudenmire, The ITensor software library for tensor network calculations, *SciPost Phys. Codebases* **2022**, 4 (2022).
- [74] C. K. Majumdar and D. K. Ghosh, On next-nearest-neighbor interaction in linear chain. I, *J. Math. Phys.* **10**, 1388 (1969).
- [75] C. K. Majumdar and D. K. Ghosh, On next-nearest-neighbor interaction in linear chain. II, *J. Math. Phys.* **10**, 1399 (1969).
- [76] M. Schreiber, S. S. Hodgman, P. Bordia, H. P. Lüschen, M. H. Fischer, R. Vosk, E. Altman, U. Schneider, and I. Bloch, Observation of many-body localization of interacting fermions in a quasirandom optical lattice, *Science* **349**, 842 (2015).
- [77] J. Zhang, P. W. Hess, A. Kyprianidis, P. Becker, A. Lee, J. Smith, G. Pagano, I.-D. Potirniche, A. C. Potter, A. Vishwanath, N. Y. Yao, and C. Monroe, Observation of a discrete time crystal, *Nature (London)* **543**, 217 (2017).
- [78] B. Synak-Radtke and M. Horodecki, Classical information deficit and monotonicity on local operations, *J. Phys. A: Math. Gen.* **37**, 11465 (2004).